Int. J. Electrochem. Sci., 15 **(2020)** 11594 – 11605, doi: 10.20964/2020.11.42

International Journal of
ELECTROCHEMICAL
SCIENCE
www.electrochemsci.org

Short Communication

Comparison of Ethanol Gas Sensors based on PbS nanoparticles and Bulk PbS

*A.K. Mishra, S.*Saha

Department of physics, Vidyasagar University, Paschim Medinipur, West Bengal, PIN 721102, India
*E-mail: anjanmishra2011@gmail.com

Received: 22 May 2020 / *Accepted:* 4 September 2020 / *Published:* 30 September 2020

An attempt is made to fabricate the ethanol gas sensor at room temperature. A cost-effective and simple chemical reduction route is used to grow cubic and spherical PbS nanoparticles using Ethylene Diamine as a capping agent. Bulk PbS is grown by a simple chemical method without using any capping agent. Structural characterization of samples is done by X-ray diffraction (XRD), transmission electron microscopy(TEM), and scanning electron microscopy(SEM). Optical characterization is done by UV-Visible-NIR absorption spectroscopy. The gas sensor is fabricated based on cubic, spherical PbS nanoparticles, and bulk PbS. Sensitivity measurement is done at room temperature for ethanol gas by three types of sensors. Ethanol gas Response, Response time, and Recovery time are calculated for different shapes of PbS nanoparticles and bulk PbS. Gas sensitivity is found to be high for sensor-based on spherical PbS nanoparticles and is less for sensors based on bulk PbS.

Keywords: Lead Sulfide, Nanoparticles, X-Ray diffraction, Gas Sensor, Ethanol, Sensitivity.

1. INTRODUCTION

More sensors require high operation temperature (200-600°C) and high power consumption for fast response [1, 2]. Any leakage of highly flammable and toxic chemicals creates environmental hazards. Ethanol gas sensors have several applications in chemical, biomedical, food technology, and also in monitoring drunken driving [3]. There are so many methods for ethanol gas sensors and techniques for sensor fabrication [4–7]. Sensors are fabricated based on Sn-doped ZnO [8], ZnO nanowires [9], CuO film [10], SnS2 nanoflakes [11], ZnO nanorods [12], ZnO nanoparticles [13], and PbS nanomaterials [14]. SnS_2, ZnS, CdS, Ag_2S, PbS are used in photo-detecting and gas sensing applications [15–17,40-53]. Lead sulfide is a typical p-type semiconductor with a narrow bandgap energy of 0.5 eV at room temperature [18]. PbS nanoparticles have a large surface to volume ratio and highly tunable in geometric dimension. Due to low costs and large-area production, PbS nanoparticles are well suited in gas sensor sensitivity. PbS nanoparticles are able to detect ammonia gas [19], Liquified

Petroleum Gas [20], Hydrogen Sulfide Gas [21], and Nitrogen dioxide [22]. L. D. Bharatula et al [23] prepared SnS_2 nanoflakes by the chemical process. They measured gas sensing response for different alcohol and confirmed the highest selectivity to methanol. Whereas the response was measured 211 for 150 ppm concentration of ethanol at room temperature. P. S. Kuchi et al [24] fabricated an ethanol gas sensor made from Cuo NPs decorating by ZnO Nps synthesized by the Solvothermal method. They found that ethanol gas sensing response was 97 to 200 ppm of ethanol and 300 to 2000 ppm of ethanol at 320℃. N. K. Pawar et al [25] prepared nano Fe_2O_3 film by screen printing technique and gas sensing performance was studied for CO, CO_2, NH_3, H_2, Cl_2, ethanol, LPG, H_2S. Prepared nano Fe_2O_3 film showed the highest sensitivity to ethanol gas at 350℃ temperature at 250 ppm concentration with short response time and large recovery time.

Two different shape PbS nanoparticles are grown with Ethylene Diamine as a capping agent. Bulk PbS is grown without using any capping agent. Three gas sensors are made for two different shapes PbS nanoparticles and bulk PbS. The ethanol gas sensing performances of the prepared sensor was done at room temperature. Ethanol gas sensing efficiency, Response time, and Recovery time for three fabricated gas sensors are compared.

2. EXPERIMENTAL SECTION

2.1 Preparation of PbS nanocrystals and bulk PbS

The method of preparation for PbS nanoparticles and bulk PbS were different. Ethylene Diamine was used as a solvant for reaction medium in PbS nanoparticle formation. PbS nanoparticles were grown using reagents Lead chloride, Sulfur powder, Sodium borohydride for two different molar ratio as 1:1:1 and 1:1:3. Ethylene Diamine was used as a capping agent. Sodium borohydride was used as a reducing agent to initiate the reaction between Lead chloride and Sulfur powder.The two different reactions were performed with two different reducing agent ratio for preparation of PbS nanoparticles.

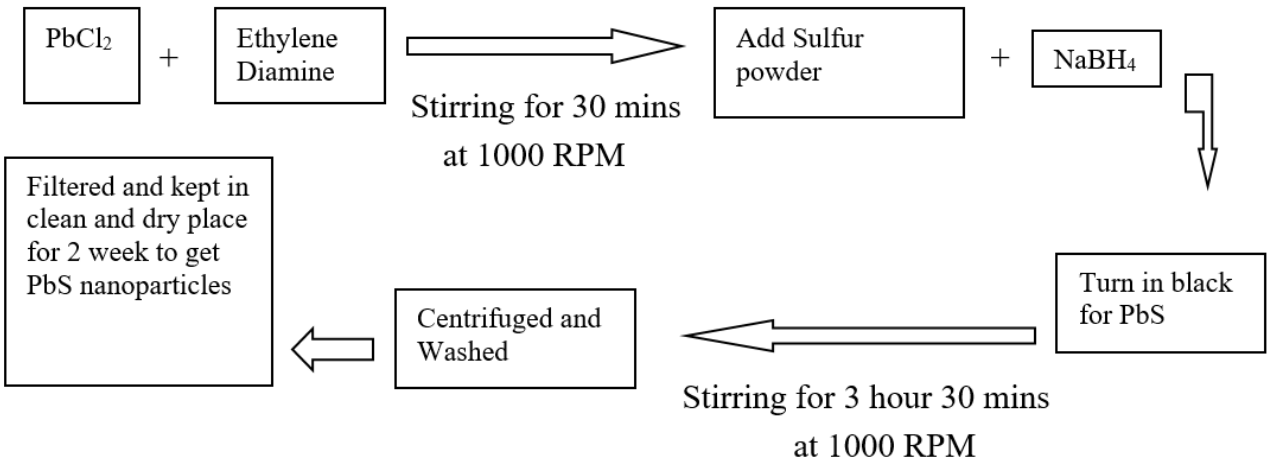

The PbS nanoparticles with 1:1:1 molar ratio were grown using 2.75 gm lead chloride, 0.32 gm sulfur, 0.037 gm sodium borohydride, and 50 ml Ethylene Diamine in a beaker. The PbS nanoparticles

with 1:1:3 molar ratio were grown using 2.75 gm lead chloride, 0.32 gm sulfur, 1.11 gm sodium borohydride, and 50 ml Ethylene Diamine. Both reactions were occurred by following the same procedure according to flowchart given above. The reaction mechanism for PbS nanoparticle formation is given below

$PbCl_2 = Pb^{+2} + 2Cl^-$

$NaBH_4 + Cl^- = NaCl + B_2H_6 + 2H^+ + 2e^-$

$2H^+ + S^{-2} = H_2S$

$H_2S + Pb^{+2} + 2e^- = PbS + H_2$

The bulk PbS was grown using two reagents with 1:1 molar ratio. And for bulk PbS no capping agent was used. Reagents were Lead acetate and Thiourea. The reaction is occurred in a medium maintaining pH value around 11 adding NH_4OH as a complexing agent. In the chemical bath deposition method,S^{-2} ion generation and the reaction rate is managed by the influence of pH. PbS samples are grown with less stoichiometric for lower pH (<11) but the ratio of product composition of Pb^{+2} and S^{-2} is about 1:1 for pH value (~11) [38,39].

Bulk PbS was formed in the chemical bath deposition method when the product of cations and anions concentration value exceeds the solubility product. Lead acetate [$Pb(CH_3COO)_2$] released Pb^{+2} ions and thiourea [$CS(NH_2)_2$] dissociated into SH^- ions due to the addition of NH_4OH in aqueous solution. Then the reaction occurred with SH^- ion, and OH^- ion to give S^{-2} ion. Finally, this Pb^{+2} cations combined with S^{-2} anions to give PbS. The reaction process for bulk PbS formation is given below.

$Pb(CH_3COO)_2 = Pb^{2+} + 2CH_3COO^-$

$(NH_2)_2C=S + OH^- = CH_2N_2 + H_2O + SH^-$

$SH^- + OH^- = S^{-2} + H_2O$

$Pb^{+2} + S^{-2} = PbS$

2.2. PbS samples characterization

X-ray diffraction (XRD) patterns of powder PbS samples are obtained from the High-resolution Rigaku Mini Flex X-ray diffractometer. All samples are taken for range 20 to 80 degrees. TEM images of PbS samples are taken by JEOL-JEM 2100 HRTEM. Selected area electron diffraction (SAED) pattern is taken which confirms the polycrystalline nature of PbS sample. The surface morphology of the samples is studied from the scanning electron microscopy(SEM). After ultrasonication of PbS samples in ethanol medium, absorption spectra are obtained by Agilent Technologies Cary 5000 Series UV-VIS-NIR Spectrophotometer.

2.3 Sensor fabrication

At first, three cutting glass slides were ultrasonicated in ethanol for 30 min each to get rid of the stain from glasses. For ethanol gas sensor fabrication two different size PbS nanoparticles and bulk PbS samples are deposited on clean glass by a spin coating method. And finally, silver electrodes (separated by 1cm each other) were painted on three different PbS glass films using brass for electrical contacts.

2.4 Sensor characterization

Very few PbS nanosensors have been checked selectivity. PbS nanosensor quality parameter like response time, recovery time, dynamic range, linearity, detectivity, lifetime, and operational parameter reproducibility, transportability, cost should be checked for sensor device made of nanomaterials as well as bulk material and compared. For sensor characterizations of PbS samples, voltage and current in the circuit were measured by Keithley 4200 scs electrical parameter analyzer.

3. RESULT AND DISCUSSION

3.1 Structural Characterisation

The XRD pattern of different PbS nanoparticles and bulk PbS are shown in Fig.1

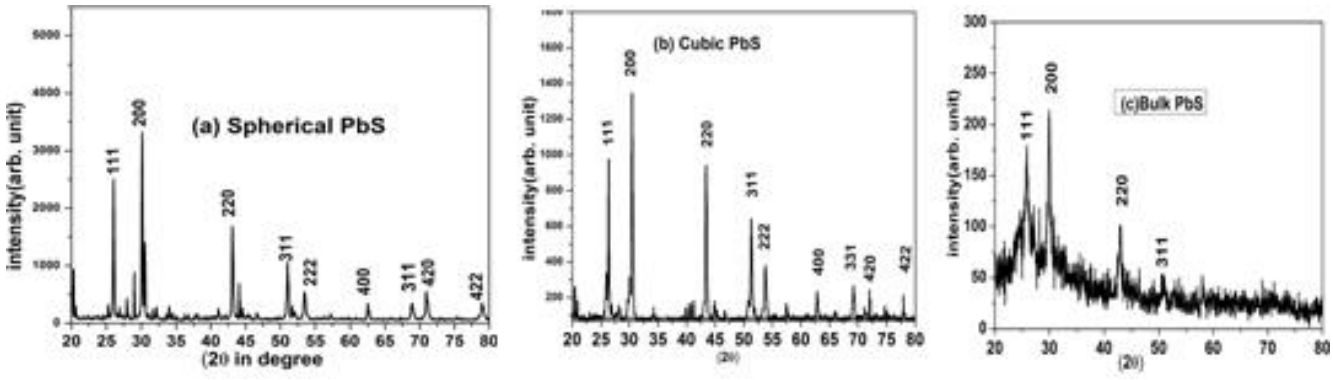

Figure 1. XRD pattern of (a) spherical PbS nanoparticles (b) cubic PbS nanoparticles (c) bulk PbS.

With standard JCPDS database, XRD data shows crystallinity along (200) direction nine diffraction peaks (111), (200), (220), (311),(222),(400), (331), (420) and (422)were identified in XRD pattern of PbS nanoparticles. Four diffraction peaks (111), (200), (220) and (222) were identified in the XRD pattern of bulk PbS. XRD pattern confirms the formation of face-centered cubic PbS nanoparticles. The obtained XRD data shows high phase purity and crystallinity along 200 direction. The size of PbS samples obtained from the Debye-Scherrer equation $D=0.9\ \lambda/(bCOS\theta)$ where D is particle size in nm, λ is the X-ray wavelength in nm, θ is the diffraction angle in degrees and B is the maximum peak width in half-height. The average particle size calculated from the diffraction pattern is the almost same result for TEM pictures.

TEM images of different shape PbS nanoparticles, bulk PbS are shown in Fig.2.

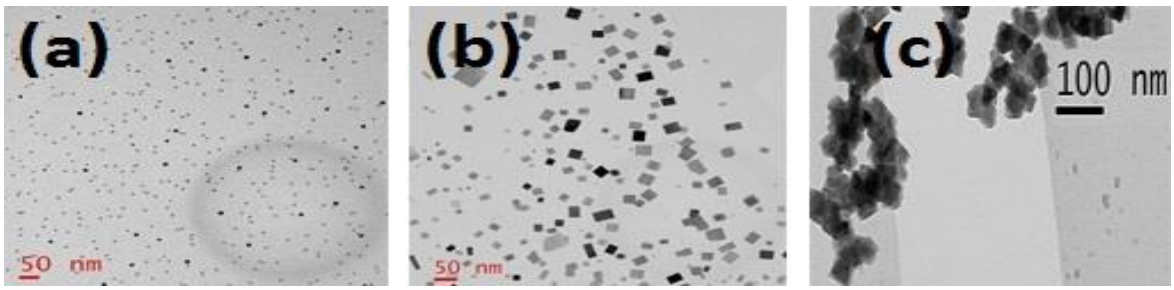

Figure 2.TEM images of (a) spherical PbS nanoparticles (b) cubic PbS nanoparticles (c) bulk PbS.

The size of spherical PbS nanoparticles is obtained 7 nm from the TEM pictures. The average particle size cubic shapes PbS nanoparticles is calculated 10 nm and the size of bulk PbS is found 45 nm. The spherical and cubic shaped nanoparticles of PbS show good isolation in the TEM pictures.

SEM images of different shape PbS nanoparticles, bulk PbS are shown in Fig.3.

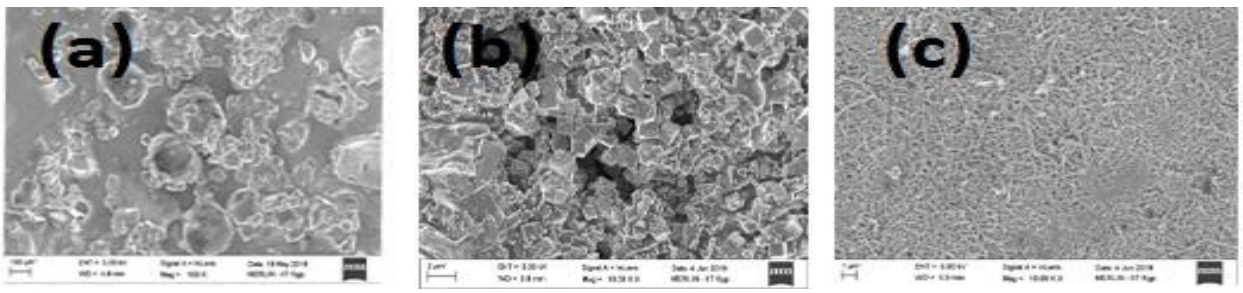

Figure 3. SEM images of (a) spherical PbS nanoparticles (b) cubic PbS nanoparticles (c) bulk PbS.

We get different surface morphology for different shape PbS nanoparticles are shown in fig 3 and for bulk PbS it is fibrous one.

3.2 Optical characterization

Optical absorption spectra of different shape PbS nanoparticles and bulk PbS are shown in Fig.4.

For PbS samples optical absorption is done in the NIR region. Optical absorption data for PbS samples are taken in the wavelength range of 1000 to 2000 nm. The bandgap of PbS nanoparticles and bulk PbS is determined using the relation is given by $(\alpha h\gamma)^2 = K(h\gamma - E_g)$ where K is a constant, E_g is the bandgap energy, h is Planck's constant, α is the absorption coefficient, and ɣ is the frequency of the photon. Photon energy (hυ) with $(\alpha h\upsilon)^2$ is plotted in Fig.5.

Optical absorption spectra of Spherical PbS, cubic PbS nanoparticles, and bulk PbS are shown in Fig4.

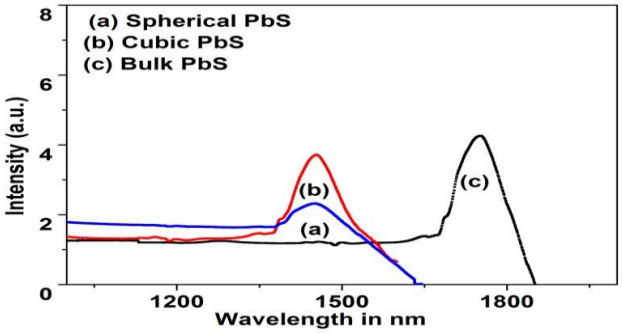

Figure 4. Optical absorption spectra of (a) spherical PbS nanoparticles (b) cubic PbS nanoparticles (c) bulk PbS

Bandgap determination plot of Spherical PbS, cubic PbS nanoparticles, and bulk PbS are shown in Fig5.

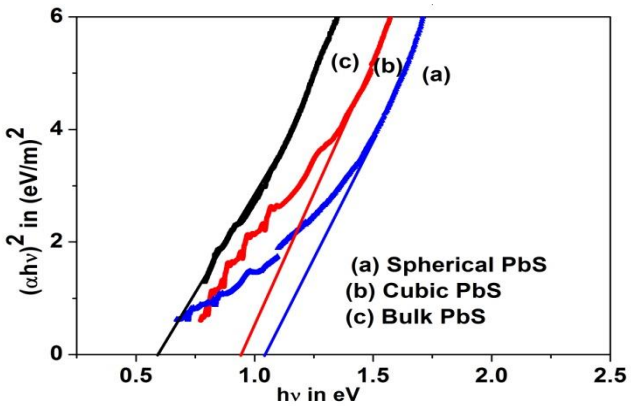

Figure 5. Bandgap determination plot of (a) spherical PbS nanoparticles (b) cubic PbS nanoparticles and (c) bulk PbS.

Band gaps of the Spherical PbS, Cubic PbS NPs are 1.03 eV, 0.93 eV, and while for bulk PbS, it is 0.59 eV.

3.3. Gas sensing properties

The gas measurement chamber is purged by keeping in the presence of artificial air for 30 min for getting better baseline resistance before every measurement. The resistance of gas sensor decreases on exposure to oxidizing gases such that NO_2, Cl_2, and resistance of gas sensor increase on exposure to reducing gases such that H_2S, ethanol, methanol, and ammonia due to p-type PbS samples [26]. The selectivity of the ethanol gas sensor is defined by the ability to respond to ethanol gas in the presence of air. To study selectivity of gas sensors based on PbS nanoparticles and bulk PbS, sensing performance were studied for 100 ppm gas concentration at room temperature of oxidizing Cl_2, NO_2, and reducing gas H_2S, CH_3OH, and C_2H_5OH. It is confirmed that gas response to reducing gas C_2H_5OH is maximum

at room temperature whereas it is quite small for other gases. Hence it confirmed the selectivity to ethanol gas at room temperature for gas sensors based on PbS nanoparticles and bulk PbS.

PbS gas sensor resistance increases on exposure to reducing gas ethanol. The inorganic material shows changes due to adsorption oxygen from the air as the O_2^-, O^- and O_2 species. The adsorption of oxygen occurs in three different away based on temperatures. At the temperature below 150 ℃, oxygen has O_2^-character, in the temperature between 150 ℃ and 400 ℃ oxygen has O^- character, and the temperature above 400 ℃ oxygen has character O^{-2} [27]. The ethanol gas sensitivity mechanism by PbS samples is given below. The effect of different concentrations of ethanol gas on the response of different shape PbS nanoparticles and bulk PbS gas sensor is studied by measuring the change of the sensor's electrical resistance. This shows that the highest sensitivity is observed for ethanol gas sensor based on spherical PbS nanoparticles.

The sensitivity of the gas sensor for different shape PbS nanoparticles, bulk PbS are shown in Fig.6.

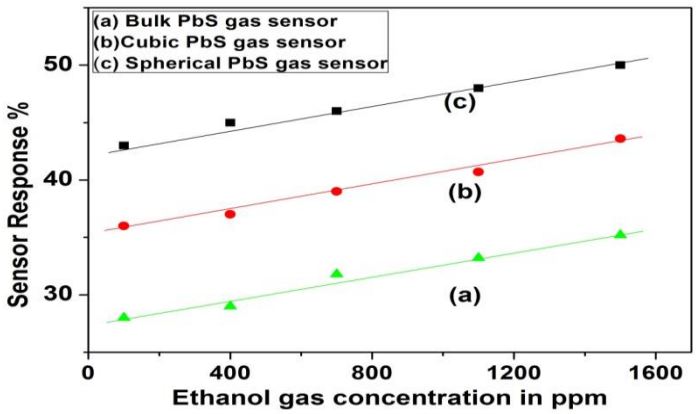

Figure 6. The sensitivity of the gas sensor for (a) bulk PbS (b) cubic PbS nanoparticles (c) spherical PbS nanoparticles.

We calculate gas sensor's response as the percentage of the resistance deviation at gas exposure (*Rg*) from the resistance in clean air (*Ra*) S%= $\{(R_g - R_a)/R_a\} \times 100\%$ Response time is defined as the time taken by the sensor to reach 90 % of the total change in sensor resistance when it is exposed to target gas and the recovery time is the time required for the reverse process after gas removing of the test chamber. All experiments were performed at room temperature (25ºC).

Resistance variation of the gas sensor for different shapes PbS nanoparticles, bulk PbS are shown in Fig.7

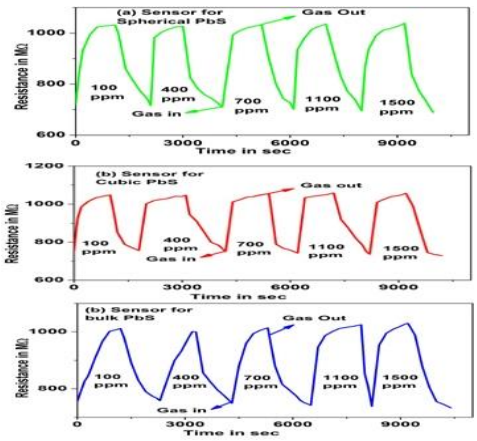

Figure 7. Resistance variation for gas sensors based on (a) spherical PbS nanoparticles (b) cubic PbS nanoparticles (c)bulk PbS for ethanol at room temperature.

Table 1. Response and recovery time of gas sensor for (a) spherical PbS nanoparticles (b) cubic PbS nanoparticles (c) bulk PbS for 100 to 1500 ppm ethanol.

		100ppm	400ppm	700ppm	1100ppm	1500ppm
Response Time	(a)Spherical PbS nanoparticles	461	439	424	373	322
	(b)Cubic PbS nanoparticles	529	515	507	484	380
	(c) Bulk PbS	650	620	605	550	470
Recovery Time	(a)Spherical PbS nanoparticles	455	434	410	342	316
	(b)Cubic PbS nanoparticles	524	509	500	459	370
	(c) Bulk PbS	564	520	530	470	390

Recovery Time and Response time is small for spherical PbS nanoparticles while it is larger for bulk PbS.

The sensor response was checked at room temperature for four weeks.

The stability of ethanol gas sensor for different shape PbS nanoparticles and bulk PbS for 100 ppm ethanol for 4 weeks are shown in fig 8.

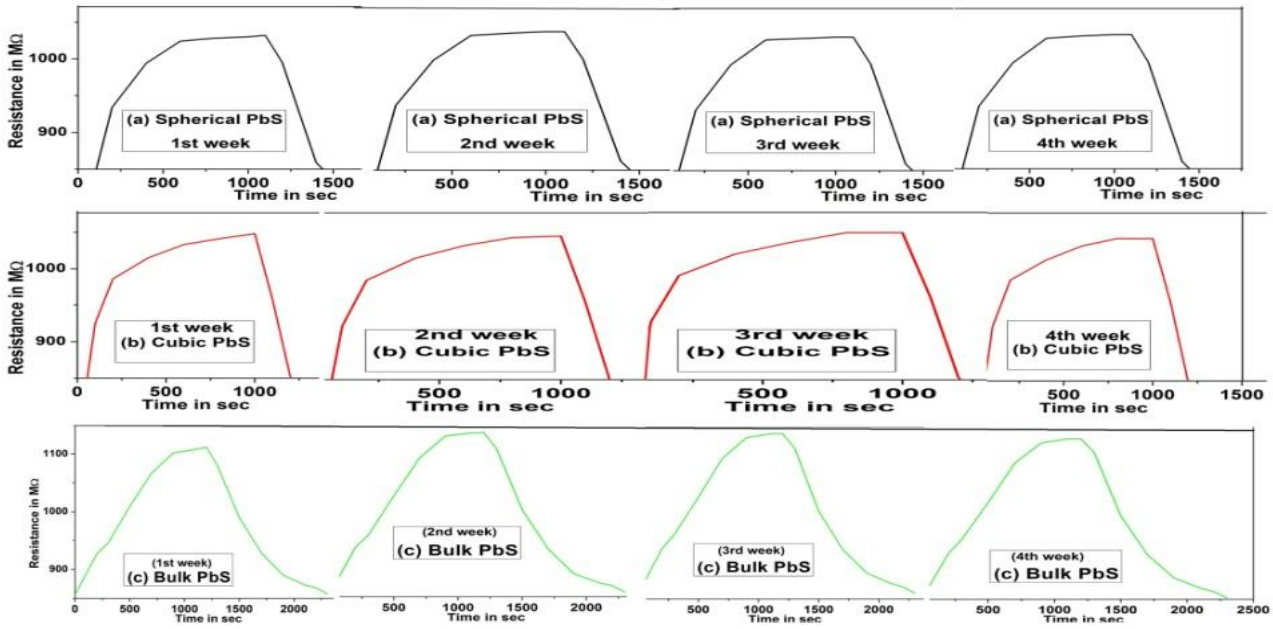

Figure 8. Stability of ethanol gas sensor for (a) spherical PbS nanoparticles (b) cubic PbS nanoparticles (c) bulk PbS for 100 ppm ethanol for 4 weeks.

Gas sensing response is higher for high reaction rate coefficient and low electron concentrations. PbS is a p-type semiconductor. PbS gas sensor in air medium adsorbs O_2 molecules. These O_2 molecules become O_2^- ions due to electron capture from PbS surface. Wolkenstein's model explanation is followed.

O_2 (gas) + e$\longrightarrow$ (O_2^-) ads

So electrons are captured by such oxygen from the PbS samples surface and this decrease in electron concentrations in PbS sample produces a positive charge region by holes. PbS sample's surface layer is covered with negative ions. Hence decreasing in sensing resistance for PbS sensor is observed and after saturation is established its value becomes constant. When PbS sensors are exposed to ethanol gas, trapping of gas molecules by the sensors with adsorbed O_2 layers are happened. Water is formed by H^+ coming from ethyl group combining with OH^- group as well as adsorbed oxygen and desorbs by giving a single electron. Decreasing in hole density in PbS sample as well as negative charge in the surface layer may be due to electron-hole pair annihilation by adsorbing ethanol gas on the surface of PbS sensor. Hence sensing the resistance of PbS sensors increases. The sensing reaction is given below

C_2H_5OH (g) + $3O_2^-$ +3 hole$\rightarrow$ $2CO_2$ (g) + $3H_2O$(g)

A comparison of the response of ethanol gas sensor based on PbS nanoparticles and bulk PbS with previous ethanol gas sensor Table2.

Samples	Year	Synthesis of nanoparticles	Temp. (℃)	Gas conc. (ppm)	Response	Ref.
ZnO/SnO_2	2013	Electrospinning	300		23	28

SnO_2	2015	Molecular imprinting	300	100	19	29
CuO	2016	Spray pyrolysis	150	300	45	30
PbS	2016	Hydrothermal	400	10-300	3.04	31
SnO_2-RGO	2017	Microwave	RT	50-1500	2-11.5	32
ZnO/SnO_2	2017	Hydrothermal	225	0.5-100	78.2	33
SnO_2/Zn_2SnO_4	2018	Hydrothermal	250	100	30.5	34
ZnO/SnO_2	2019	Spray pyrolysis	400	25	50	35
Sn doped α-Fe_2O_3	2020	Nano-casting	280	100	45.5	36
α-$Bi_2Mo_3O_{12}$/Co_3O_4	2020	Electrospinning	170	100	30.25	37
PbS nanoparticles	2020	Simple cost-effective Chemical bath deposition	RT	100-1500	43-50	This work

4. CONCLUSION

Different shape PbS nanoparticles are grown by varying ratios of reagents Lead Chloride, Sulfur powder, and $NaBH_4$. PbS nanoparticles become spherical for 1:1:1 reagent ratio and for 1:1:3 particles are cubic shape. Ethylene Diamine acts as a capping agent. But for bulk PbS there is no such capping agent used. Ethanol gas sensor constructed from spherical PbS nanoparticles shows a high dynamic range, high sensitivity, and short response time, a high dynamic range, high sensitivity, and short response time, short recovery time compare to bulk PbS. The response of the spherical PbS sensor was 43-50% for 100-1500 ppm of ethanol gas at room temperature. Thus spherical PbS nanoparticles based gas sensor shows most efficiency compared to cubic PbS nanoparticles and bulk PbS. Thus shape and size of PbS samples are the factors to sensitivity, selectivity, and stability of ethanol gas sensor based on PbS.

References

1. H. Liu, M. Li, O. Voznyy, L. Hu, Q. Fu, D. Zhou, Z. Xia, E. H. Sargent, J. Tang, *Advanced Materials*, 66 (2014)1-7. DOI:10.1002/adma.2013043.
2. J.K. Park, H.J. Yee, K.S. Lee, W.Y. Lee, M.C. Shin, T.H. Kim, S.R. Kim, *Anal. Chim.Acta*, 390 (1999) 83–91. doi:10.1016/S0003- 2670(99)00135-X.
3. M. Lakhane, R. Khairnar, M. Mahabole*, Bull.Mater.Sci.,* 39 (2016) 1483–1492.doi:10.1007/s12034-016-1286-8.
4. P. Shankar, J.B.B. Rayappan, *J. Mater. Chem*.C.,5 (2017) 10869– 10880. DOI:10.1039/C7TC03771F
5. M. Sinha, R. Mahapatra, B. Mondal, R. Ghosh, *J. Electron.Mater*., 46 (2017) 1–7 DOI:10.1016/j.matpr.2019.03.031
6. M. Ghodrati, A. Farmani, A. Mir, *IEEE Sens*. J., 19 (2019) 7373– 7377. doi:10.1109/JSEN.2019.2916850.
7. M.S. Hosseini, S. Zeinali, M.H. Sheikhi, *Sensors Actuators B Chem*., 230 (2016) 9–16. DOI:10.1016/j.snb.2016.02.008.
8. S. Luo, Y. Shen, Z. Wu, M. Cao, F. Gu, L. Wang, *Mater. Sci. Semicond. Process*., 41 (2016) 535–

543. DOI:10.1016/j.mssp.2015.10.001.
9. Z.Q. Zheng, J.D. Yao, B. Wang, G.W. Yang, *Sci. Rep*., 5 (2015) 11070. DOI:10.1038/srep11070
10. X. Liu, Y. Sun, M. Yu, Y. Yin, B. Du, W. Tang, T. Jiang, B. Yang, W. Cao, M.N.R. Ashfold, *Sensors Actuators, B Chem*., 255 (2018) 3384–3390. DOI:10.1016/j.snb.2017.09.165.
11. L.D. Bharatula, M.B. Erande, I.S. Mulla, C.S. Rout, D.J. Late, *RSC Adv*., 6 (2016) 105421–105427. DOI:10.1039/C6RA21252B
12. C. Li, L. Li, Z. Du, H. Yu, Y. Xiang, Y. Li, Y. Cai, T. Wang, *Nanotechnology,* 19 (2008) 035501. DOI:10.1088/0957-4484/19/03/035501
13. Q. Wan, Q.H. Li, Y.J. Chen, T.H. Wang, X.L. He, J.P. Li, C.L. Lin, *Appl. Phys. Lett*., 84 (2004) 3654– 3656. DOI:10.1063/1.1738932.
14. M. Yu, G. Suyambrakasam, R. Wu, M. Chavali, *Mater. Res. Bull.,* 47 (2012) 1713–1718. doi:10.1016/j.materresbull.2012.03.046
15. S. Bandyopadhyay, B. Chatterjee, P. Nag, A. Bandyopadhyay, CLEAN - Soil, *Air, Water*, 43 (2015) 1121–1127. DOI:10.1002/clen.201400437
16. I.Hwang, M. Seol, H. Kim, K. Yong, Appl. Phys. Lett., 103 (2013). DOI:10.1063/1.4813445.
17. S. Singh, A. Singh, B.C. Yadav, P. Tandon, S. Kumar, R.R. Yadav, S.I. Pomogailo, G.I. Dzhardimalieva, A.D. Pomogailo, *Sensors Actuators, B Chem*., 207 (2015) 460–469. DOI:10.1016/j.snb.2014.10.047.
18. K. Xu, N. Li, D. Zeng, S. Tian, S. Zhang, D. Hu, C. Xie, *Mater. An*., 7 (2015) 11359–11368. DOI:10.1021/acsami.5b01856.
19. C. Song, M. Sun, Y. Yin, J. Xiao, W. Dong, C. Li, L. Zhang, *Mater. Res*. 19 (2016) 1351–1355. DOI:10.1590/1980-5373-mr-2015-0683
20. Y. Liu, L. Wang, H. Wang, M. Xiong, T. Yang, G.S. Zakharova, *Sensors Actuators B Chem*., 236 (2016) 529–536. DOI:10.1016/j.snb.2016.06.037.
21. S.V. Patil, P.R. Deshmukh, C.D. Lokhande, *Sensors Actuators B Chem*., 156 (2011) 450–455. DOI:10.1016/j.snb.2011.04.005.
22. H. Liu, M. Li, G. Shao, W. Zhang, W. Wang, H. Song, H. Cao, W. Ma, J. Tang, *Sensors Actuators* B Chem., 212 (2015) 434–439. DOI:10.1016/j.snb.2015.02.047.
23. Y. Kim, D. Phan, S. Ahn, K. Nam, C. Park, K. Jeon, *Sensors Actuators B Chem*., 255 (2018) 616–621. DOI:10.1016/j.snb.2017.08.091
24. L.D. Bharatula, M.B. Erande, I.S. Mulla, C.S. Rout, D.J. Late*, RSC Adv.* 6 (2016) 105421–105427. DOI:10.1039/C6RA21252B
25. P. S. kuchi1, H. Roshan1, M. H. Sheikhi1, *Journal of Alloys and Compounds* (2019), DOI: https://doi.org/10.1016/j.jallcom.2019.152666.
26. N.K. Pawar, D.D.Kajale, G.E.Patil,V.G.Wagh,V.B. Gaikwad, M.K.Deore,G.H. Jain, *Int. J. Smart Sens. Intell.Syst*.,5 (2012) 441–457.doi:10.21307/ijssis-2017-489.
27. S. T.Navale, D. K.Bandgar, M. A. Chougule, V. B. Patil, *RSC Advances, 5(9)* (2015) *6518 6527.* doi:10.1039/c4ra15644g.
28. N.Barsan, U. Weimar, *J. Electroceram*. 7 (2001)143–167.
29. E.Nikan, A. A. Khodadadi, Y. Mortazavi, *Sensors, and Actuators B: Chemical* 184 (2013) 196–204.
30. W. Tan, Q. Yu, X. Ruan, X. Huang, *Sensors and Actuators B: Chemical* 212 (2015) 47-54.
31. M.L. Zeggar, F. Bourfaa, A. Adjimi, M.S. Aida, N. Attaf, IOP Conf. Ser.Mater.Sci.Eng.108 (2016) 012004. DOI:10.1088/1757-899X/108/1/012004.
32. C.Song, M.Sun, Y.Yin, W.J. XiaoDong, C.Li, L.Zhang, *Materials Research, 19(6)* (2016) *1351–1355.* doi:10.1590/1980-5373-mr-2015-0683
33. C.A. Zito, D.P. Volanti, Int. Conf. Adv. Ceram. Compos., (2017) pp. 271 279.doi:10.1002/9781119321811.ch25
34. J.Liu, T.Wang, B.Wang, , P. Sun, , Q.Yang, , X.Liang, G. Lu, *Sensors and Actuators B: Chemical, 245,* (2017).*551–559.* doi:10.1016/j.snb.2017.01.148.

35. X. Yang, H.Li, T. Li, Z. Li, W. Wu, C. Zhou, G.Lu, *Sensors, and Actuators B: Chemical*, (2018) DOI:10.1016/j.snb.2018.11.070.
36. T.Tharsika, M.Thanihaichelvan, A. S. M. A. Haseeb and S.A.Akbar, *Frontiers in Materials*. 6 (2019) 122.
37. J. N. Mao, B. Hong, H. D. Chen, M. H. Gao, J. C. Xu, Y. B. Han, Y. T. Yang, H. X. Jin, D. F. Jin, X. L. Peng, J. Li, H. L. Ge, X. Q. Wang, *J. Alloys Compd.*, 827 (2020) 154248.
38. S. U. Din, M. U. Haq, R. Khatoon, X. Chen, L. Li, M. Zhang, L. Zhu *RSC Adv*., 10 (2020) 21940–21953.
39. A.N.Chattarki, S. S. Kamble, L. P. Deshmukh, *Materials Letters, 67(1)* (2012) *39–41.* DOI:10.1016/j.matlet.2011.08.105
40. A.Popa, M.Lisca, V.Stancu, M.Buda, E.Pentia, T.Botila, *J Optoelectron Adv Mater*;8 (2006) 43.
41. A.K.Bhunia, T. Kamilya, S. Saha, *ChemistrySelect***,** *1* (18) (2016) 5768-5778. https://doi.org/10.1002/slct.201600973
42. A.Mohammad , J. Mazumde**r**, Int. J. Electrochem. Sci., 11 (2016) 4050 – 4075
43. J. Antonio Cruz-Navarro, Fabiola Hernandez-Garcia, A.Giaan, A. Romero, *Coordination Chemistry Reviews* https://doi.org/10.1016/j.ccr.2020.213263
44. J. Rodrigues, M. Hoppe, N. B. Sedrine, N. Wolff, V. Duppel, L. Kienle, R. Adelung, Y. K. Mishra, M. R. Correia, T. Monteiro, *Nanoscale Adv.,* 2 (2020) 2114–2126.
45. R. Bhattacharya, T. K. Das, S. Saha, *Journal of Materials Science: Materials in Electronics*, 22 (2011) 1761–1765.
46. X.Liu, T.Ma, N.Pinna, J. Zhang, *Advanced Functional Materials, 27(37)* (2017). *1702168.* DOI:10.1002/adfm.201702168
47. M. Li, W. Zhang, G. Shao, H. Kan, Z. Song, S. Xu, H. Yu, S. Jiang, J. Luo, H. Liu, *Thin Solid Films,* 618(B)1 (2016) 271-276.
48. P. Mehta, S.Vedachalam, G.Sathyaraj, S. Garai, G. Arthanareeswaran, K. Sankaranarayanan, *Journal of Molecular Liquids*,305 (2020) 112820.
49. F.Chouikh, Y.Beggar, N.Tabet, N.Ariche, M.S.Aida, *Materials Science in Semiconductor Processing,* 64(15) (2017) 39-46.
50. M. W. Jung, S. Myung, W. Song, M.A. Kang, S. H. Kim, C.S. Yang, S. S. Lee, J. Lim, C.Y. Park, J.O. Lee, K.S. An**,** *ACS Applied Materials & Interfaces*, 6(16) (2014) 13319-13323.
51. Q. Zhang, C. An, S. Fan, S. Shi, R. Zhang, J. Zhang, Q. Li, D. Zhang, X. Hu, J. Liu, *Nanotechnology,* 29 **(**2018) 285501.
52. J. Huang, Y. Dai, C. Gu, Y. Sun, J. Liu, *Journal of Alloys and Compounds*, 575(25) (2013) 115-122.
53. P.N.Li, A.V.Ghule, J.Y.Chang, *Journal of Power Sources* 354, (30) (2017) 100-107.
54. H. Roshan, M. H. Sheikhi, M. Kazem, F. Haghighi, *IEEE Sensors Journal,* 20(5) (2020) 1.